Local Hemodynamics and Intimal Hyperplasia at the Venous Side of a Porcine Arteriovenous Shunt

Themistoklis A. Manos, Dimitrios P. Sokolis, Athina T. Giagini, Constantinos H. Davos, John D. Kakisis, Eleftherios P. Kritharis, Nikos Stergiopulos, Panayotis E. Karayannacos, Sokrates Tsangaris

***Abstract*—Venous anastomotic intimal hyperplasia (IH) observed in the arteriovenous shunt (AVS) has been associated with disturbed hemodynamics. This study aims to correlate hemodynamics with wall histology and wall mechanics by examining the flow field in AVS with computational fluid dynamics using experimental data taken from in vivo experiments. Input data to the computational model was obtained in vivo one month later; adjacent vessels were submitted to histological and mechanical examination. The 3D shunt geometry was determined using biplane angiography. Ultrasound measurements of flow rates were performed with perivascular flow probes and pressures were recorded through intravascular catheters. This data was considered as boundary conditions for calculation of the unsteady flow field. Numerical findings are suggestive of strong Dean vortices towards both vein flow exits, verified by color Doppler. The high wall shear stresses and their gradients appear to be related to areas of IH and vessel wall stiffening, as evidenced in preliminary histological and mechanical studies of the venous wall. Additionally, suture line hyperplasia seems to be aggravated by the high wall shear stress gradients noted at the transition line from graft to vein.**

***Index Terms*—Arteriovenous Shunt, Computational Fluid Dynamics, Doppler Ultrasound, Hemodynamics, Intimal Hyperplasia, Swine Model.**

Manuscript is a modified and enhanced version of the paper presented in IEEE BIBE 2008 in Athens, Greece. This paper is part of the 03ED 262 research project, implemented within the framework of the "Reinforcement of Human Research Manpower" (PENED) and co-financed by National and Community Funds (20% from Greek Ministry of Development – General Secretariat of Research and Technology and 80% from E.U. – European Social Fund).

T. A. Manos is with the Laboratory of Biofluid-Mechanics and Biomedical Engineering, National Technical University of Athens, Athens, Greece (e-mail: tmanos@fluid.mech.ntua.gr).

D. P. Sokolis is with the Center of Experimental Surgery, Foundation of Biomedical Research, Academy of Athens, Athens, Greece (e-mail: dsokolis@bioacademy.gr).

A. T. Giagini is with the Center of Experimental Surgery, Foundation of Biomedical Research, Academy of Athens, Athens, Greece (e-mail: atgiag@bioacademy.gr).

C. H. Davos is with the Clinical Research Center, Foundation of Biomedical Research, Academy of Athens, Athens, Greece (e-mail: cdavos@bioacademy.gr).

J. D. Kakisis is with the Vascular Unit, 3rd Department of Surgery, University of Athens School of Medicine, Attikon University Hospital, Athens, Greece (e-mail: kakisis@yahoo.gr).

E. P. Kritharis is with the Laboratory of Biofluid-Mechanics and Biomedical Engineering, National Technical University of Athens, Athens, Greece (e-mail: leyterisk_4@hotmail.com).

P. E. Karayannacos is with the Center of Experimental Surgery, Foundation of Biomedical Research, Academy of Athens, Athens, Greece (e-mail: pkarayannacos@bioacademy.gr).

N. Stergiopulos is with the Laboratory of Hemodynamics and Cardiovascular Technology, Swiss Federal Institute of Technology, Lausanne, Switzerland (e-mail: nikolaos.stergiopulos@epfl.ch).

S. Tsangaris is with the Laboratory of Biofluid-Mechanics and Biomedical Engineering, National Technical University of Athens, Athens, Greece (corresponding author, e-mail: tsanga@central.ntua.gr, 0030-210-7721043; fax: 0030-210-7721057).

I. Introduction

THE arteriovenous shunt (AVS) is the surgical connection of an artery to a vein through a graft, creating an access site for chronic hemodialysis therapy in patients with end stage renal disease [1]. Over the past decades, the number of AVS procedures has steadily risen in both Europe and the United States, and is expected to rise steeply in the near future, owing to the ongoing global diabetes epidemic. Polytetrafluroethylene (PTFE) is the most commonly used hemodialysis access graft material, yet their current patency rate at two years is 25% due to the formation of intimal hyperplasia (IH) at the venous side of AVS [2]. Surgical intervention may thus be necessary within two to three years, representing a major socio-economic burden.

A multitude of factors have been proposed to predispose to graft occlusion and failure, the most important being mechanical injury of the host vein, mismatched compliance between graft and vein, and unphysiological hemodynamic conditions in the peri-anastomotic region, i.e. turbulent flow [3], regions of high wall shear stress (WSS) [3]-[5], high WSS gradient [6], and oscillatory WSS [7] (see reviews in [8]-[10]). Nevertheless, no unanimous agreement exists to date as to the hemodynamic stimulus principally responsible for the development of focal stenoses in the venous outflow tract of AVS grafts.

Toward that end, our paper presents a combined in vivo and numerical study, aiming at examining the hemodynamic factors associated with anastomotic IH in AVS. A subject-specific geometry in an animal model was employed together with boundary conditions obtained from in vivo flow and pressure measurements. Our numerical results were correlated with

histology, color Doppler ultrasound, and wall mechanics. Past reports [6], [11]-[14] have mostly studied idealized geometries of AVS and only one study [15] documents this kind of data association so far, but with numerical and histological data from different animals. Our findings may facilitate our understanding of the pathophysiology of hemodialysis access complications.

II. Materials and Methods

A. Animal Model

A healthy male Landrace pig weighing 65 kg underwent creation of an AVS between the carotid artery and jugular vein via an expanded (e-PTFE) graft, according to the model by Rotmans et al. [16]. Animal housing and handling complied with the guiding principles of the American Physiological Society and the 160/1991 Greek Presidential Decree, issued after the 609/1986 European Union Directive. The protocol was approved by the Ethics Committee of Foundation of Biomedical Research.

B. Surgical Procedures

Six days preoperatively, the animal was administered acetylsalicylic acid (100 mg/day), clopidogrel (75 mg/day), and digoxin (25 mg/day) until termination; the latter stopped on the 8th day postoperatively. On the day of surgery, it was sedated with intramuscular ketamine (10 mg/kg), azaperone (4 mg/kg), and atropine (0.05 mg/kg). Anaesthesia was induced with intravenous administration of propofol (0.9 mg/kg). Sevoflurane 3-5 % (vaporizer setting) in oxygen was administered for maintenance of anesthesia.

Under sterile conditions, a midline cervical incision was made, and the right common carotid artery and ipsilateral internal jugular vein were exposed. Papaverine (5 mg/ml) was instilled locally to avoid vasospasm. Heparin (iv, 200 IU/kg) was given before manipulation of the vessels. The artery was clamped using atraumatic clamps and an 8-mm arteriotomy was performed. An end-to-side anastomosis was created at a 45º angle using continuous 8-0 polypropelene suture. A reinforced, thin-walled, ringed, e-PTFE graft of 6-mm diameter and 10-cm length was used (Advanta VS; Atrium Medical Corp). The venous anastomosis was created similarly, Fig. 1.

C. Euthanasia and Tissue Preparation

One month postoperatively, the midline neck incision was reopened, and both jugular veins were carefully exposed. Flow, pressure, and diameter measurements were conducted as described below. The in situ length of both veins (proximal vein segments (PVS), Fig. 1) was determined by measuring the distance between two surgical knots. The animal was sacrificed with a bolus dose of pentobarbital sodium, the anastomosed and contralateral tissues (serving as control) were excised, and their ex situ lengths measured. Adherent tissue was trimmed and specimens were prepared for geometrical study. A ring was obtained from the PVS, placed in a Petri dish with Krebs-Ringer solution, and photographed to visualize the no-load geometry by a digital camera (model E400; Olympus Optical Co) coupled to a stereomicroscope (Stemi 2000C; Carl Zeiss Optical). Ring cross-sectional area measurement was conducted on the digitized photo via Sigma Scan Pro 5 software (Aspire Software International). The left over specimens were kept for histological studies.

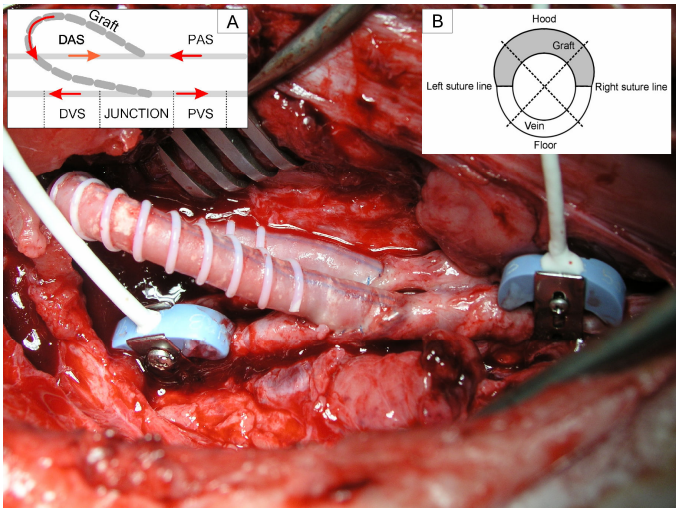

Fig. 1. AVS via an e-PTFE graft between the common carotid artery and ipsilateral internal jugular vein prior to animal euthanasia with inset: A) showing a schematic representation for the definition of specimens: (PAS, DAS) = (proximal, distal) arterial segment; (PVS, DVS) = (proximal, distal) venous segment and B) the histological cross-section at the junction region divided into four quadrants for a more detailed analysis.

D. Hemodynamic Measurements

Before euthanasia and under sedation, the flow field of the anastomosis was inspected transcutaneously with a cardiovascular color flow Doppler ultrasound system (Vivid 7; GE Medical Systems), using its linear array vascular probe (size 12L) at color and pulse wave Doppler modes. Blood flows at the proximal (PAS) and distal arterial segments (DAS), and at the proximal (PVS, Fig. 2) and distal vein segments (DVS) were measured via perivascular ultrasonic flow probes (Transonic Systems) of appropriate size (Fig. 1).

Blood flows and pressures were recorded first at the vein and then at the artery. Recordings were performed under hemodynamically stable conditions, presumably when pressures and flows did not exhibit temporal variations for about 5 min. Instantaneous diameter and pressure was recorded simultaneously at the PVS of anastomosed and contralateral veins. Proximal venous pressure was measured through a 5F catheter-tipped pressure transducer (SPC-450; Millar Instruments) and a pair of sonometrics piezoelectric crystals (Sonometrics Corp) glued on the tissue measured external diameter using principles of ultrasonography. All signals were recorded by a Sonometrics data acquisition system (Sonometrics Corp) at 60-sec data epochs with a sampling rate in excess of 300 Hz, during which the respirator was turned off to avoid respiration-induced noise.

E. Biplane Angiography

After hemodynamic measurements, biplane angiography was carried out using a C-arm mobile diagnostic X-ray system (BV

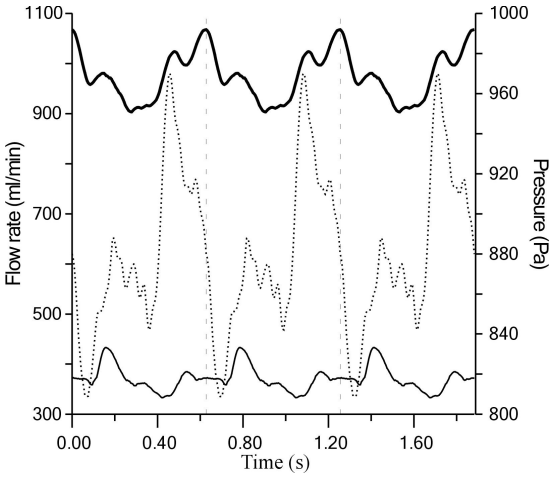

Fig. 2. Processed recordings of flow rate at the graft inlet (top thick line), of pressure (dotted line) at DVS, and of flow rate (bottom thin line) at PVS were all used as boundary conditions for the computational model.

Libra; Philips Medical Systems). A catheter was inserted into the graft and the C-arm tested at various angles to avoid adjustments during image acquisition. Iobitridol (658.1 mg/ml) contrast media was administered and digital subtraction angiography was performed at three pre-selected angles, allowing unambiguous identification of the venous anastomosis. The monitor output was recorded on DVD, Fig. 3 (left).

F. Histomorphometrical Studies

To examine the regional distribution of morphometric parameters in the venous segments of AVS, vein tissue for histological study was cut into four parts: the DVS, heel and toe of junction, and DVS (Fig. 1) that were afterwards subdivided into four quadrants with respect to circumferential position; these referred to the hood, floor, left and right lateral suture line for the junction region, and similarly for the PVS and DVS, as has been performed in PTFE end-to side arterial anastomoses by Loth et al. [17]. Specimens were fixed with 10% buffered formalin over 24 hours and embedded in paraffin. Serial 5-μm thick sections were cut on a microtome (Leica RM 2125; Leica) and treated with picro-Sirius red for collagen matrix and orcein for elastin fiber staining. Images were taken by a digital camera (Altra 20; Soft Imaging System), fitted to a light microscope (Olympus CX3; Olympus), and processed with commercial software (Image-Pro Plus v.6.0; Media Cybernetics Inc). The thickness of tunica intima, media, and adventitia was measured. Elastin and collagen contents for all layers were also measured after micrograph segmentation, with respect to the total area of that layer in the region of interest. Values for each specimen were averages from three sections.

G. Postoperative Data Editing and Analysis

Data stored in Sonometrics acquisition system was used as boundary conditions. The flow rates at the PAS and DAS were added to obtain graft inlet flow (Fig. 2) and the same was done at the PVS and DVS. Pressure and flow signals were delineated according to cardiac cycle. Synchronization of the recordings performed first at the venous and then at the arterial side of AVS was achieved by a reference signal, i.e. the flow through the graft. A characteristic cardiac pulse was selected and extracted. Data analysis was carried out with Sonosoft software (Sonometrics Corp). All signals were filtered to remove the linear drift produced by temporal variations of hemodynamics at the anastomosis.

Graft and DVS flows, and PVS pressure were selected for processing in MATLAB, serving as boundary conditions to our model. This data was re-sampled based on a common time vector, and then smoothed and curve-fitted using a Fourier fit of eighth degree. A user defined function programmed in C, defining pressure and flow for every time step, was subsequently used as input for the unsteady numerical simulation.

H. Determination of Mechanical Properties of Vein Wall

The internal diameter d_i of PVS was calculated from external diameter d_e, measured in vivo, the in situ longitudinal extension of vein λ_z, and the cross-sectional area A_0 of wall at excision, assuming constancy of tissue volume for a cylindrical vessel: $d_i = \sqrt{d_e^2 - 4A_0/\pi\lambda_z}$. Lumen area-pressure data was fitted with a three-parameter (α, β, and γ) arctangent model: $A = \pi d_i^2/4 = a\left[\pi/2 + tan^{-1}\left(P - \beta/\gamma\right)\right]$. Local venous area compliance C was calculated as the first derivative of lumen area with respect to pressure and distensibility D as compliance normalized by lumen area. Owing to the nonlinearity of area-pressure data, both decrease with inflating pressure. To determine these indices for a given level of blood pressure, compliance-pressure and distensibility-pressure curves were determined over the systolic-diastolic range. Analyses were performed on ten consecutive cycles and the results averaged.

I. Reconstruction of Geometry and Mesh Development

All angles, at which the monitor output was recorded, were studied and appropriate images were selected for geometrical reconstruction. Using the Info Cliper software (Canopus Co), images of interest were captured. Venous anastomosis was planar in the case studied, its plane being perpendicular to the surgical table. There was thus no need for a reconstruction algorithm; only one image at an axis vertical to the plane of anastomosis was required, Fig. 3 (left). The chosen image was rotated, filtered, and segmented using Image-Pro Plus software. The vessels centerline and boundaries were traced manually by point selection with Paint Shop Pro 5 (Jasc Software Inc). This modified image was processed by a developed MATLAB code that extracted the coordinates of selected points. The point cloud was imported into GAMBIT (v.2.3.16; Fluent Inc). The 3D geometry was reconstructed assuming circular cross-sections of varying diameter for the graft and vessel. The model was cut in the middle, taking into account planar symmetry, reducing the total number of elements. Geometry was split into four regions: i.e., the junction, PVS, DVS, and graft inlet. An unstructured grid was used in the junction, comprising wedge, tetrahedral, and pyramidal elements, and a structured grid with hexahedral elements for the other three volumes, Fig. 3 (right). The total element count was 173177.

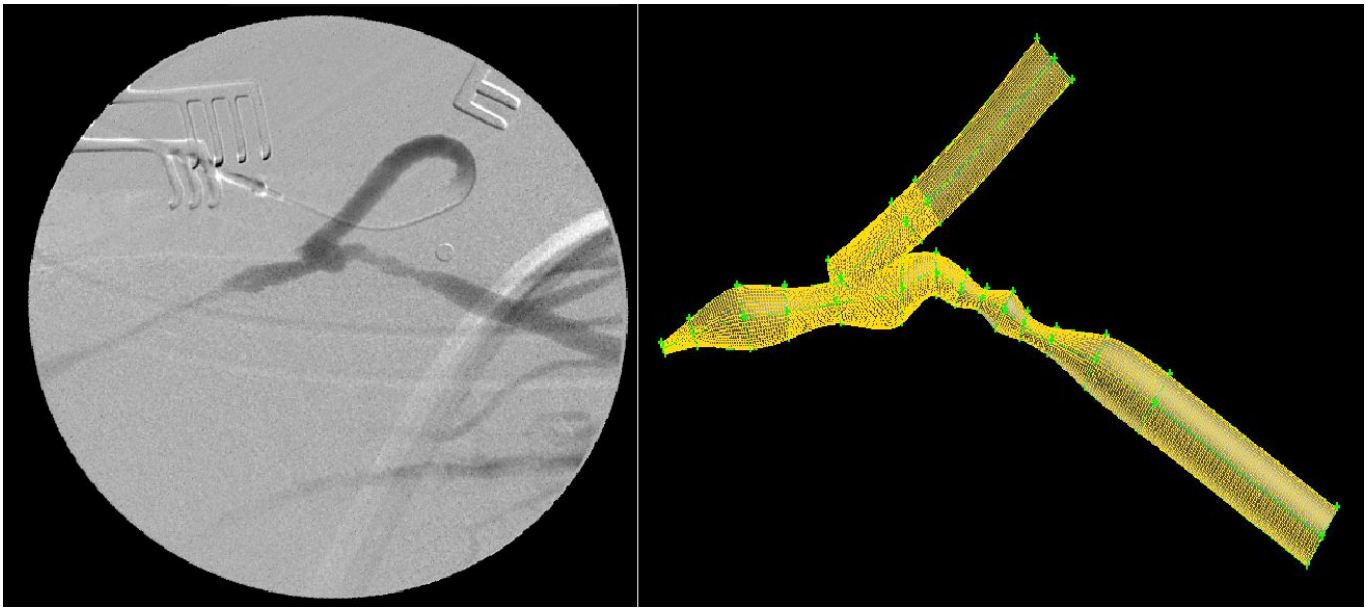

Fig. 3 Angiography (left) and 3D mesh of graft-vein anastomosis generated by GAMBIT (right) for a selected time point of the cardiac cycle, based on curve fits.

J. Numerical Simulation

The mesh generated was exported to the finite volume solver Fluent (v.6.2.16; Fluent Inc). Blood was approximated as a Newtonian fluid with viscosity of 3.6×10^{-3} Pa s and density of 1000 kg/m^3. Flow was assumed to be laminar and pulsating. The processed recordings of pressure and flows were taken as boundary conditions (Fig. 2). Pulsatile entrance velocities with plug profiles were applied at the graft inlet and PVS, and the time dependent pressure waveform at the DVS. The boundary condition temporal variation was set according to the aforementioned user defined function, which was coupled to the solver. The mean flow rate was 980 ml/min, corresponding to mean graft inflow velocity of 0.47 m/s or mean Reynolds number of 870, based on the graft inlet diameter, with the highest Reynolds number being 952. The pulse period, about 0.63 s (heart rate of 95 bpm), was divided into 100 time steps; three cycles were initially simulated to eliminate transient artifacts.

The Navier-Stokes equations were solved using a segregated solver with a first-order implicit unsteady formulation, while a PRESTO! scheme was used for pressure and a first-order upwind scheme for momentum discretization. The pressure-velocity coupling method of choice was the PISO algorithm. Convergence criteria, defining the end of the iterative process, were continuity and momentum residuals of 0.0001.

When convergence was achieved, the computational results were exported to Tecplot (Tecplot Inc) and the instantaneous normalized WSS gradient ($WSSG_{ND}$) was calculated. The WSS gradient (WSSG) was normalized by the ratio of the mean Poiseuille WSS at the graft inlet divided by graft diameter. The gradient was calculated for the maximum flow case, since the inlet's flow variation was small and the maximum $WSSG_{ND}$ is considered most hazardous [6], [9].

III. Results

A. Numerical Simulation Results

The flow patterns observed were complex and highly 3D, due to the irregular geometry of AVS one month post-surgery. The velocity vectors at the symmetry plane are shown in Fig. 4 [A, B]. Flow entered the graft as a plug velocity profile, but became fully developed approaching the host vessel. Part of the flow, before entering the junction region, collided with the wall of the bulge that was present near the toe section and a recirculation zone evolved at that point. In contrast, the main part of flow struck the floor of host vessel and separated into two streams of opposite directions (Fig. 4 [A, B]). A stagnation point formed at the point of division.

Following that part of the stream heading towards the PVS exit, we found that as it turned on the flow dividing wall, it set up a Dean flow pattern in which flow on the lateral walls moved upwards towards the toe, Fig. 4 [C]. These counter rotating vortices had their center near the toe wall at start, approaching the vessel axis downstream. At the PVS exit, there was a vessel constriction; maximum flow velocities ranging from 4.9 to 5.0 m/s during the cardiac cycle were noted there. The flow field pattern did not display significant temporal variation.

The other part of inlet flow, which divided at the stagnation point, moved towards the DVS exit. This stream also formed Dean vortices (Fig. 4 [D]), accompanying it until it reached the exit, except with a diminishing effect. DVS exhibited two stenotic regions lying close to each other. The first created a strong jet stream that passed through the expansion zone between the two stenoses and entered the final one. High velocities between 1.8 and 2.3 m/s were detected at these stenotic areas. The two expansion zones caused flow separation

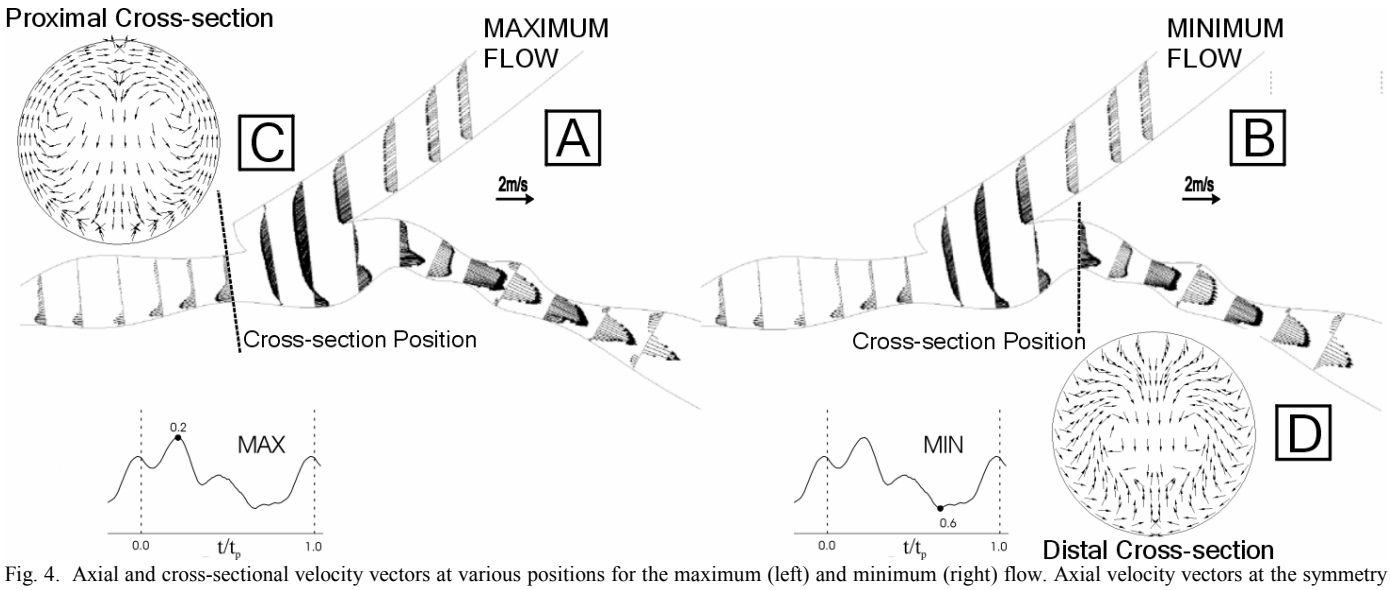

Fig. 4. Axial and cross-sectional velocity vectors at various positions for the maximum (left) and minimum (right) flow. Axial velocity vectors at the symmetry plane for the maximum [A] and minimum [B] flow, illustrating the existence of recirculation zones in the DVS. Unscaled, cross-sectional velocity vectors at the PVS [C] for maximum flow and the DVS [D] for minimum flow near the junction, depicting Dean vortices.

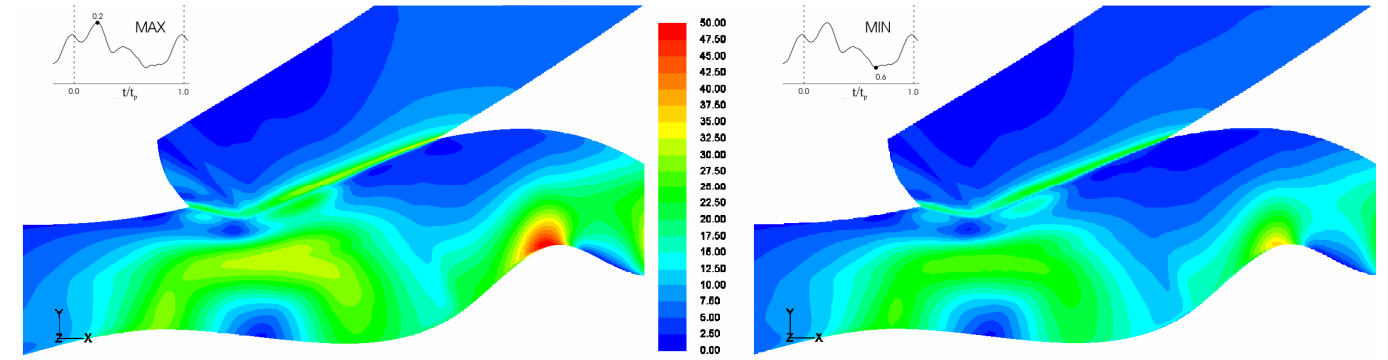

Fig. 5. WSS contours emphasizing the large temporal increase opposite to the heel. Maximum (left) and minimum inlet flow rate (right).

and as a consequence recirculation zones formed that altered during the cardiac cycle. For the minimum graft inlet flow, the jet was longer and produced a large recirculation zone with combined Dean vortices on the top of the second expansion area, whereas at the bottom a simple recirculation region of smaller scale slowly emerged (Fig. 4 [B]). In contrast, for the maximum inlet flow the jet was shorter yet with higher velocities, causing two extended recirculation zones, but with Dean flow apparent only for the bottom one, which increased in size becoming the largest of the two (Fig. 4 [A]).

WSS contours at the junction region are displayed in Fig. 5 for the maximum (left) and minimum (right) flow cases. The mean value of WSS calculated was 6.0-7.5 Pa, consistent with the value reported by Harugushi et al. [9]. The maximum value was found at the stenosis of the PVS exit, between 680 and 696 Pa. Other regions of high WSS were the first, i.e. 93-124 Pa, and second stenosis, i.e. 68-89 Pa, of the DVS, the floor of the DVS opposite to the heel region, i.e. 33-49 Pa, and finally the region around the stagnation point on the lateral walls of the host vessel, i.e. 27-31 Pa.

The above mentioned range of WSS values and Fig. 5 illustrate a regional dependence of temporal variation among the PVS and DVS. The PVS and junction region exhibited slight changes in WSS, in contrast to DVS, where greater alterations were noted, especially on the venous floor opposite the heel. The difference was caused by temporal change in flow division during the cardiac pulse. For minimum inlet flow, a 44:56, whereas for maximum flow a 38:62 PVS:DVS flow split was observed. This means that as graft flow increased more blood was channeled away from the PVS, which was partially occluded. As a result the flow rate increase, defining WSS variation, was 2% and 28% for the PVS and DVS, respectively; meaning that the DVS was subjected to higher temporal WSS gradients.

Information on the spatial variation of WSS is provided by $WSSG_{ND}$ contours (Fig. 6). Results showed that the highest values existed at the PVS stenosis (~4950), then at the floor of first DVS stenosis (~3000), and finally at the junction; for most other regions the $WSSG_{ND}$ was much lower, so that its mean value was approximately 70 (Fig. 6 [A]). The highest values observed at the junction region were those at the heel (~2450), although high values reaching 900 were also noted along the suture lines and toe (Fig. 6 [B]).

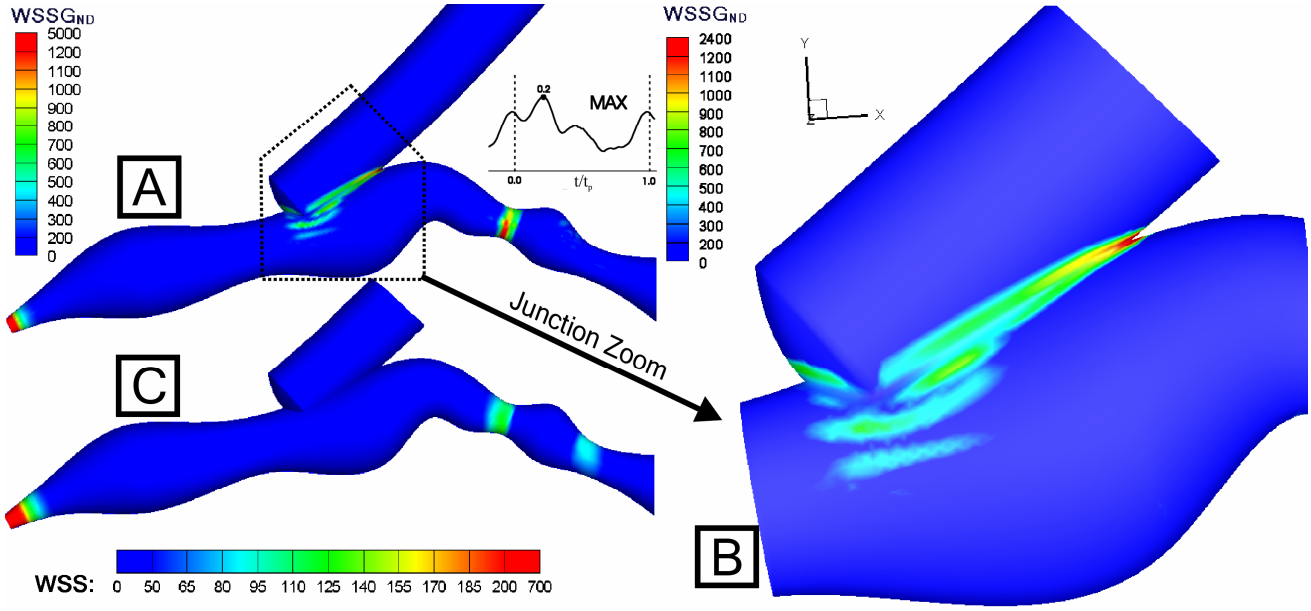

Fig. 6. WSSG$_{ND}$ contours for the whole model [A] and the junction region only [B]. Also in the same figure, for comparison reasons, the corresponding whole model WSS contours [C] were also displayed. Note: In order to depict the variations in more detail the contour levels for extremely low and high values were shown with only one level and no color change, while for WSSG$_{ND}$ values ranging between 200-1200 [A and B] and WSS between 50-200 Pa [C] there was a uniform distribution.

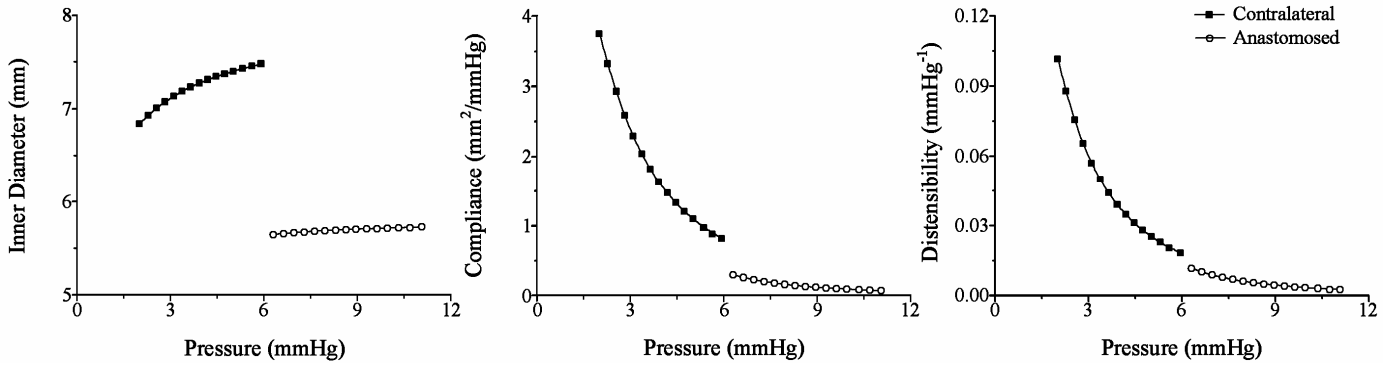

Fig. 7. Inner diameter (left), compliance (middle), and distensibility (right) vs. pressure curves of contralateral (control) and anastomosed (grafted) jugular veins (PVS).

B. Mechanical Properties of Vein Wall

The diameter-pressure curve (Fig. 7 left) of the anastomosed PVS was shifted towards lower levels of diameter and higher pressures, following a different line of elasticity than that of the contralateral segment. The mechanical adaptation of anastomosed vein tissue was assessed via structural, e.g. compliance and distensibility, parameters. The compliance-pressure curve of the anastomosed vein decayed exponentially over the systolic-diastolic range, exhibiting lower values than control (Fig. 7 middle). A similar trend was noted in the respective distensibility-pressure curves (Fig. 7 right). At each mean venous pressure, decrease in the two parameters was found in anastomosed than control vessels.

C. Histomorphometrical Properties of Vein Wall

Fig. 8 summarizes our histomorphometrical results. No circumferential variations were noted in control tissue, and parameters from the four quadrants were pooled. An increase in layer thickness of anastomosed than control vein was noted at all segments. The media and adventitia exhibited less striking variations among the different quadrants and segments, while intima suffered considerable thickening, attesting to IH [16], [18]. The greatest intima thickness increase was noted at the DVS, followed by the heel and toe of the junction, and the PVS (Fig. 8). At the DVS, intima thickness was homogeneously distributed in the various quadrants, consonant with our numerical findings of high velocities, WSS, and WSSG in this topographic segment. At the heel of the junction, the peak intima thickness was found in the suture lines between graft and vein, and similar was the case at the toe, but with lower values than the heel. At the PVS, an even lower intima thickness was observed similarly so in all quadrants. As regards elastin content, there was a decline in all tunicas of anastomosed tissue

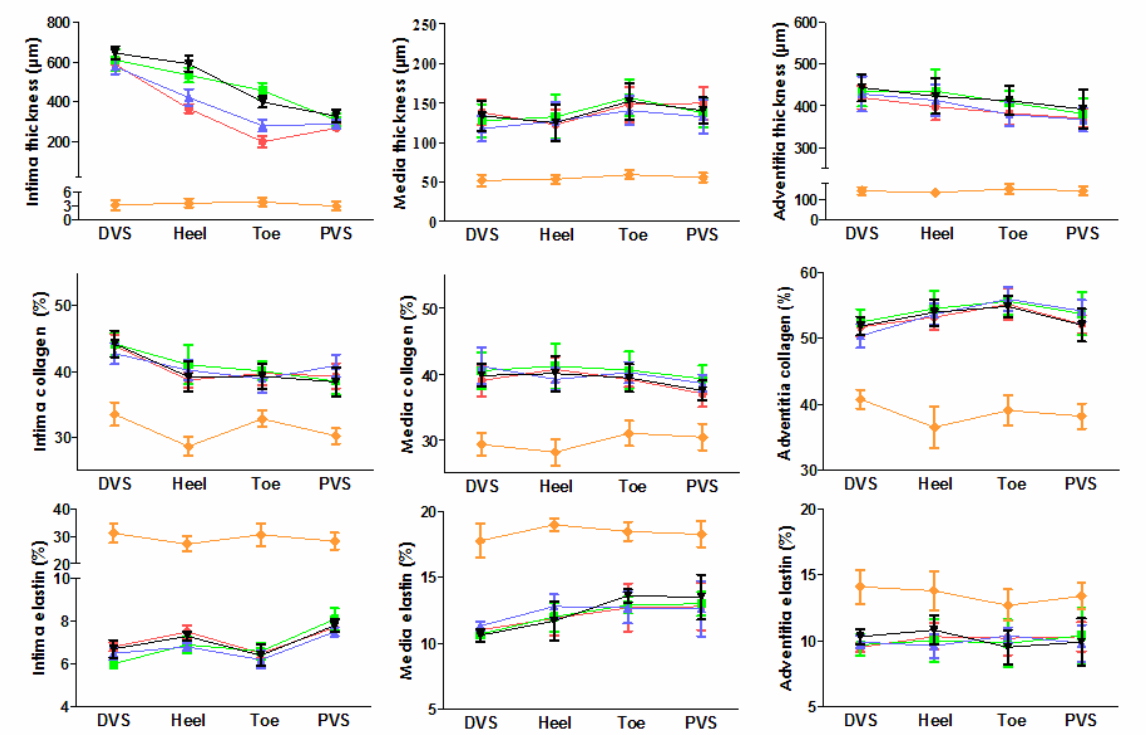

Fig. 8. Thickness (upper panel), collagen content (middle panel), and elastin content (lower panel) of intima, media, and adventitia at the DVS, heel and toe of junction, and PVS of anastomosed and control veins. Line color defines the quadrant used for the measurement: red (hood), light green (right suture line), blue (floor) and black (left suture line). Control tissue showed no circumferential variation that is why only one orange line is displayed for this case.

in all quadrants (Fig. 8). This is in agreement with the literature, according to which areas of high velocities and WSS correlate with reduced elastin content [16], [19]. Elastin content reduction was less marked at the PVS compared to the other segments, without circumferential heterogeneity. Collagen results were the exact opposite to those of elastin [16], but again did not vary in the different quadrants (Fig. 8).

D. Ultrasound Results

One month postoperatively, just before reopening the neck incision, the transcutaneous ultrasound measurement was performed. During post-processing, the recorded color Doppler images exhibited Dean vortices (Fig. 9) in the form of three consecutive stripes of alternating colors (red-blue-red). The middle stripe could not be mistaken for a recirculation zone, since it extended from one side of the vessel lumen to the other.

IV. Discussion

In the present study, we found that the hemodynamics predicted by the computational model were exceptionally complex, particularly along the DVS. In this area, a jet stream was observed accompanied by recirculation zones that were sometimes coupled with Dean vortices, features not reported in previous studies [6], [11]-[15]. The basis for the differential flow characteristics was the subject-specific geometry of the porcine AVS. This was captured by biplane angiography one month post-surgery, when IH had developed, distorting the initial geometry. The geometry studied displayed several irregularities, i.e. a bulge at the toe area, a stenosis at the PVS exit, and two stenoses at the DVS. All vessel formations must have been provoked by IH, owing to the disturbed flow post-AVS.

The long-term effect of AVS creation on vein histology of a single animal was assessed in this study, supporting the widely-reported IH in grafted veins. Most thickening occurred in the intimal layer, and there was collagen fiber accumulation at the expense of elastin. Morphometric data on the same animal model have been given by Rotmans et al. [16], [19]; still, control tissue thickness was not evaluated and measurements were confined to the intima and media. They noted IH and elevated intima to media ratio that was aggravated over time. Their data on extracellular matrix composition of the entire vessel revealed a reduction in elastin content, in line with this study, but a more pronounced increase in collagen content. Importantly, we have documented the circumferential variation of IH in different regions that has not been presented earlier, allowing for a more exact correlation with hemodynamics.

Numerous hemodynamic factors have been incriminated to predispose to hemodialysis access graft occlusion and failure. Among them, the markedly high WSS and turbulence may be expected to injure endothelial cells of the vein outflow tract and elicit IH by smooth muscle proliferation. As a confirmation, Hofstra et al. [5] demonstrated in hemodialysis patients a correlation of follow-up vessel stenosis, developed around the venous anastomosis or PVS, with the elevated peak systolic blood velocity immediately after AVS, and with initial relative distension, i.e. an indicator of venous strain during the cardiac cycle.

In an animal study, Fillinger et al. [3] created AVS using unbanded and banded grafts, reporting in both cases major IH

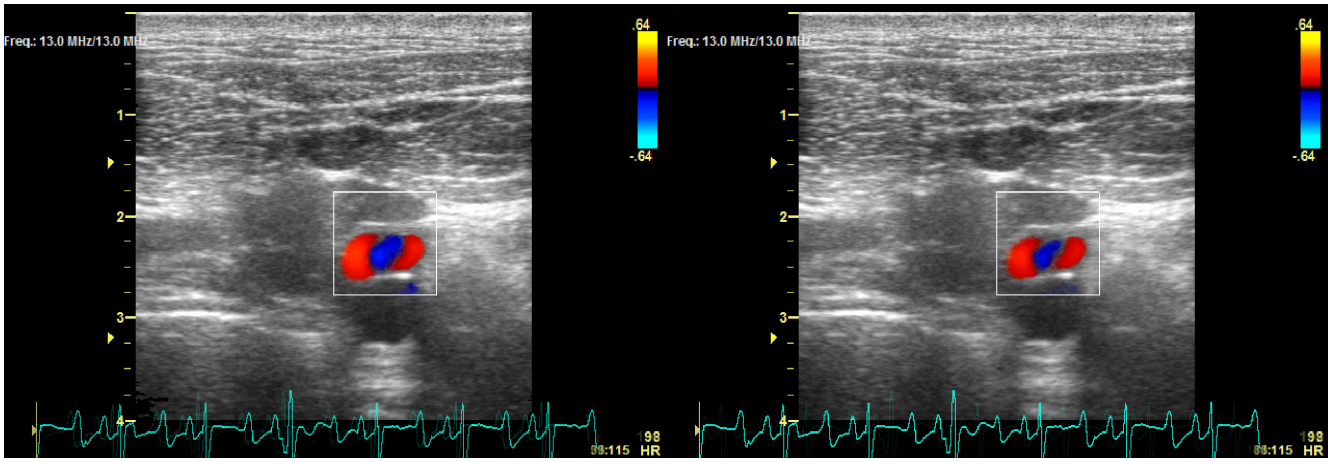

Fig. 9. Dean vortices at cross-sections obtained trancutaneously by color Doppler ultrasound. Color demonstrates the direction of velocity components parallel to the view plane. Red color exhibits flow towards, whereas blue flow away from the probe. Maximum (left) and minimum inlet flow rate (right).

close to the anastomosis and a favorable effect of banding on venous thickening that was well associated with Reynolds number. These authors inferred that turbulence is a major factor in the development of IH in AVS. That group also investigated the effect of graft geometry [4] and documented less intimal hyperplastic response when using 4-7-mm tapered grafts than straight 6-mm grafts. Clinical studies, however, showed similar blood flow rates and patency rates in tapered and untapered grafts [20]. Similar conclusions were drawn by numerical simulations, which displayed no significant hemodynamic advantage for tapered grafts [14].

Longest et al. [6] in a numerical study suggested that, although WSS distribution did indicate the existence of disturbance, further hemodynamic parameters were needed in order to detect areas of possible IH development. They attempted to overcome this problem by using the time averaged WSSG, the time averaged WSS angle gradient (WSSAG), and the radial pressure gradient (RPG). Amongst these parameters, the WSSG has found wide acceptance and has been used extensively for arterial bypass studies [8], [9], although few are the AVS studies to have used it [6], [14]. Their results displayed increased WSSG principally at the toe, which is a known region of increased IH, and to a lesser extent along the junction's lateral walls.

Our histomorphometrical results specified regional differences, with the DVS close to the heel affected the most by IH, although evidence from clinical [2], [5] and animal studies [3], [4] has shown that it usually develops near the anastomotic region and in the PVS downstream. At the DVS, there was a 173-fold thickening of tunica intima, and the elastin content was about half the one found for control. Both alterations in vessel structure are promoted by high WSS in the literature [5], [16]-[19]. Our numerical results corroborated those findings at the far PVS, but not at the toe region. The numerical simulation performed in this study showed that the highest WSS of the junction region were found at the host vessel floor opposite to the heel, at the DVS. In contrast to the literature [6], [11]-[15], the DVS did also exhibit high WSS. We believe that this may be reminiscent of the fact that after development of IH at the PVS, flow in the distal one increased, eliciting high WSS.

$WSSG_{ND}$ was also calculated on the walls of our numerical simulation (Fig. 6 [A]). Areas of high $WSSG_{ND}$, i.e. the PVS and first DVS stenoses together with the junction heel, coincided in most cases with high WSS. However, the differences in magnitude among the various locations of the model were not proportional between $WSSG_{ND}$ and WSS (Fig. 6 [C]). The junction's heel and the first DVS stenosis exhibited similar maximum $WSSG_{ND}$, while the PVS stenosis had nearly double the values (Fig. 6[A]). On the other hand, WSS at the DVS stenosis were twice as big as those at the heel, whereas at the PVS stenosis they were ten times larger (Fig. 5). Areas that differed amongst the two parameters were the junction's lateral walls (Fig. 5 & 6[B]), the sudden downward turn of the DVS (Fig. 5 & 6[A]), as well as the second DVS stenosis (Fig. 5 & 6[A]), where WSS reached high values contrary to $WSSG_{ND}$. The values reported in our study were higher than those in the other two AVS graft studies [6], [14], because the DVS had retrograde flow in our model, whereas in others it was occludedq; also, our venous anastomosis geometry was real in contrast to the idealized models used in literature.

Correlation of $WSSG_{ND}$ with histology exhibited the importance of a smooth transition from graft to vein. At the junction region, the areas of high $WSSG_{ND}$, i.e. the heel and suture lines, coincided with the increased IH. All positions were characterized by an abrupt change in velocity direction, as the flow "followed" the wall shape at the transition line from graft to vein the $WSSG_{ND}$ soared to its maximum value. It hence seems that mechanical injury may initiate suture line IH, but abnormal hemodynamics sustains the proliferative response together with the possible influence of compliance mismatch. This means that the transition from graft to vein must be as smooth as possible. Longest et al. [6], who attempted to find an optimal geometry for AVS venous side anastomosis, also focused in minimizing graft bulges and creating smoother wall curvatures.

The most interesting flow features noted were the Dean vortices that developed in both venous exits. Similar counter rotating vortices at the PVS have also been described by Krueger et al. [12], [13], while Loth et al. [15] in a combined in

vitro and numerical study, and Longest et al. [6] in a numerical study reported secondary flows of opposite direction, in which flow moved upwards in the center and towards the floor on the lateral walls. The difference in flow pattern among the studies may be ascribed to the difference in velocity magnitude and direction at the flow inlets. In our study and [12], [13], similar peak Reynolds numbers were noticed at the graft inlet, i.e. 950 and 980, accordingly, while flow during systole exited through both the PVS and DVS. In contrast, much higher inlet flows were used in [6] and [15], with Reynolds numbers of 1820 and 1300, respectively, and the DVS was assumed as blocked in the former, and as a low flow inlet in the latter study. The geometry also differed in the various studies, but the secondary flow variation may not be simply attributed to it, because when an in vitro end-to-side anastomosis was examined [21] of identical geometry to [15], but with lower Reynolds number of 130 and an outlet at the DVS, no inverse Dean vortices were observed.

We also noted secondary flows at the DVS, in disparity to all previous studies. The reason for the disparity with [6], [15] is as explained above, while for [11]-[12] it may be that more flow exited the PVS than the DVS, and that flow at the DVS changed direction during diastole, while in our study it was with varying flow rates throughout the cardiac cycle. The existence of these vortices was validated by color Doppler ultrasound (Fig. 9).

Flow unsteadiness exerted a significant influence only on DVS hemodynamics. PVS flow rate did not demonstrate the anticipated increase. Although graft flow manifested a 17% raise, PVS flow increased by a mere 2%, because flow was channeled in the opposite direction. Consequently, the DVS showed the highest velocities, WSS, and temporal WSSG in the proximity of the junction region.

The mismatched compliance between graft and vein may additionally be anticipated to augment wall stresses and have a proliferative influence on suture line IH; yet, Hofstra et al. [5] certified a negative relation between compliance mismatch and IH in patient studies, and Shu and Hwang [7] also substantiated that this is not a main issue per se in AVS. We compared the compliance and distensibility of PVS with those of the contralateral vessel (control) and found them smaller at in vivo pressures. Our data indicated a stiffening response of the anastomosed vein to the elevated pressure and flow conditions after AVS that may facilitate in long term the matching of compliance between graft and host vein. To the best of our knowledge, the biomechanical remodeling of vein wall post-AVF has not been described, while there are data for venous hypertension by Hayashi et al. [22], Monos et al. [23], and Szentivanyi et al. [24], who did not detect changes in the mechanical properties at in vivo pressures. For veins exposed to arterial circulatory conditions, Monos and Csengody [25], opposite to our results, reported lessening in incremental elastic modulus and normalization of compliance as distensibility changes were compensated by morphological ones, i.e. thickening of the vessel. On the other hand, Wesley et al. [26] transplanted canine jugular segments into arterial circuits and reported that veins became inextensible after ten months, behaving as damaged tissue. Furthermore, the vein's morphological remodeling, i.e. the lumen diameter reduction, within one month probably restores transmural stresses to their normotensive levels. The mean transmural stress σ_θ is given by Laplace's law: $\sigma_\theta = \frac{Pd_i}{2h}$, where P is lumen pressure, d_i internal diameter, and h thickness, so that upon pressure overload, stress normalization can be attained by increasing wall thickness and/or by decreasing lumen diameter. Ongoing studies from our laboratory (data not shown) suggest that at later stages of vein remodeling when the wall is adequately thick, normalizing wall stress without contribution of lumen narrowing, the lumen is enlarged normalizing the WSS as well; since WSS may only be normalized by narrowing lumen diameter, according to Poiseuille's law: $\tau = \frac{32\mu Q}{\pi d_i^3}$, where Q was mean blood flow rate and μ blood viscosity.

Importantly, the compositional modification of grafted vein reflects alterations in wall mechanical properties. Elastin and collagen are chief contributors to the mechanical response of blood vessels, with collagen being the least and elastin the most distensible element of vessel wall. Our histological findings of reduced elastin content for the PVS wall are consistent with our mechanical findings, namely of the reduced distensibility of that segment. Though we did not assess the mechanical properties of venous wall in the other segments of the anastomosis, i.e. the junction and DVS, similar or even worse distensibility characteristics are anticipated, on the basis of the amplified elastin content changes and intimal thickening observed in those regions.

In summary, this experimental study combined in vivo hemodynamics, computational fluid dynamics, histology, and wall mechanics that were all performed in the same porcine model, one month postoperatively, for a more detailed investigation of IH at the venous side of AVS. Angiography displayed the existence of one proximal and two distal stenoses. Perivascular flow probes revealed retrograde flow at the DVS, while ultrasound color Doppler detected strong Dean vortices at the shunted vein. Computational simulation calculated the WSS and $WSSG_{ND}$ and proved that the regions most affected in the proximity of the junction was the heel and the first DVS stenosis. Histological results correlated well with these findings, exhibiting increased IH at the heel and DVS. Furthermore, suture line IH appeared to be associated with augmented $WSSG_{ND}$ at the transition line between graft and vein, attesting to the need for smoother wall curvatures at the anastomosis. The study of mechanical wall properties demonstrated vein stiffening at the PVS, which corroborated with histology, i.e. intimal thickening and reduced elastin content. Finally, it should be noted that the geometry investigated portrayed the chronically remodeled AVS, just prior to loss of patency; so that we examined the progress of IH and not its stimulus.

ACKNOWLEDGMENT

The authors thank: C. A. Dimitriou for his technical support throughout the project, E. Varela for her assistance with the U/S scanning, and M. Peroulis and M. Katsimpoulas for their aid and suggestions with the surgical procedure.

REFERENCES

[1] R. L. Pisoni, E. W. Young, D. M. Dykstra, R. N. Greenwood, E. Hecking, B. Gillespie, R. A. Wolfe, D. A. Goodkin, and P. J. Held, "Vascular access use in Europe and the United States: results from the DOPPS," *Kidney Int*., Vol. 61, pp. 305-316, 2002.

[2] R. Y. Kanterman, T. M. Vesely, T. K. Pilgram, B. W. Guy, D. W. Windus, and D. Picus, "Dialysis access grafts: anatomic location of venous stenosis and results of angioplasty," *Radiology*, Vol. 195, pp. 135-139, 1995.

[3] M. F. Fillinger, E. R. Reinitz, R. A. Schwartz, D. E. Resetarits, A. M. Paskanik, and C. E. Bredenberg, "Beneficial effects of banding on venous intimal-medial hyperplasia in arteriovenous loop grafts," *Am. J. Surg.*, Vol. 158, pp. 87-94, 1989.

[4] M. F. Fillinger, E. R. Reinitz, R. A. Schwartz, D. E. Resetarits, A. M. Paskanik, D. Bruch, and C. E. Bredenberg, "Graft geometry and venous intimal-medial hyperplasia in arteriovenous loop grafts," *J. Vasc. Surg.*, Vol. 11, pp. 556-566, 1990.

[5] L. Hofstra, D. C. Bergmans, K. M. Leunissen, A. P. Hoeks, P. J. Kitslaar, M. J. Daemen and J. H. Tordoir, "Anastomotic intimal hyperplasia in prosthetic arteriovenous fistulas for hemodialysis is associated with initial high flow velocity and not with mismatch in elastic properties," *J. Am. Soc. Nephrol.*, Vol. 6, pp. 1625-1633, 1995.

[6] P. W. Longest and C. Kleinstreuer, "Computational haemodynamics analysis and comparison study of arteriovenous grafts," *J. Med. Eng. Technol.*, Vol. 24, pp. 102-110, 2000.

[7] M. C. Shu and H. Hwang, "Haemodynamics of angioaccess venous anastomoses," *J. Biomed. Eng.*, Vol. 13, pp. 103-112, 1991.

[8] F. Loth, P. F. Fischer, and H. S. Bassiouny, "Blood flow in end-to-side anastomoses," Annu. Rev. Fluid Mech., Vol. 40, pp 367-393, 2008.

[9] H. Haruguchi and S. Teraoka, "Intimal hyperplasia and hemodynamic factors in arterial bypass and arteriovenous grafts: a review," *J. Artif. Organs*, Vol. 6, pp. 227-235, 2003.

[10] P. Roy-Chaundhury, V.P. Sukhatme and A.K. Cheung, "Hemodialysis vascular access dysfunction: a cellular and molecular viewpoint," *J. Am. Soc. Nephrol.*, Vol. 17, pp. 1112-1127, 2006.

[11] P. W. Longest, C. Kleinstreuer, and J. R. Buchanan JR, "A new near-wall residence time model applied to three arteriovenous graft end-to-side anastomoses," *Comput. Methods Biomech. Biomed. Engin.*, Vol. 4, pp. 379-397, 2001.

[12] U. Krueger, J. Zanow, and H. Scholz, "Computational fluid dynamics and vascular access," *Artif. Organs*, Vol. 26, pp. 571-575, 2002.

[13] U. Krueger, J. Zanow, and H. Scholz, "Comparison of two different arteriovenous anastomotic forms by numerical 3D simulation of blood flow," *Int. J. Angiol.*, Vol. 9, pp. 226-231, 2000.

[14] I. Van Tricht, D. De Wachter, J. Tordoir, and P. Verdonck, "Comparison of the hemodynamics in 6mm and 4-7 mm hemodialysis grafts by means of CFD," *J. Biomech.*, Vol. 39, pp. 226-236, 2006.

[15] F. Loth, P. F. Fisher, N. Arslan, C. D. Bertram, S. E. Lee, T. J. Royston, W. E. Shaalan, and H. S. Bassiouny, "Transitional flow at the venous anastomosis of an arteriovenous graft: potential activation of the ERK1/2 mechanotransduction pathway," *J. Biomech. Eng.*, Vol. 125, pp. 49-61, 2003.

[16] J. I. Rotmans, E. Velema, H. J. M. Verhagen, J. D. Blankensteijn, J. J. P. Kastelein, D. P. V. de Kleijn, M. Yo, G. Pasterkamp, and E. S. G. Stroes, "Rapid, arteriovenous graft failure due to intimal hyperplasia: a porcine, bilateral, carotid arteriovenous graft model," *J. Surg. Res.*, Vol. 113, pp. 161-171, 2003.

[17] F. Loth, S. A. Jones, C. K. Zarins, D. P. Giddens, R. F. Nassar, S. Glacov, and H. S. Bassiouny, "Relative contribution of wall shear stress and injury in experimental intimal thickening at PTFE end-to-side arterial anastomoses," *J. Biomech. Eng.*, Vol. 124, pp. 44-51, 2002.

[18] S. Misra, D. A. Woodrum, J. Homburger, S. Elkouri, J. N. Mandrekar, V. Barocas, J. F. Glockner, D. K. Rajan, and D. Mukhopadhyay, "Assessment of wall shear stress changes in arteries and veins of arteriovenous polytetrafluoroethylene grafts using magnetic resonance imaging," *Cardiovasc. Intervent. Radiol.* Vol. 29, pp. 624-629, 2006.

[19] J. I. Rotmans, E. Velema, H. J. M. Verhagen, J. D. Blankenstejin, D. R. V. Kleijn, G. Pasetrkamp, and E. S. G. Stroes, "Matrix metalloproteinase inhibition reduces intima hyperplasia in a porcine arteriovenous-graft model," *J. Vasc. Surg.*, Vol. 39, pp. 432-439, 2004.

[20] R. Dammers, R. N. Planken, K. P. Pouls, R. J. Van Det, H. Burger, F. M. Van der Sande, and J. H. Tordoir, "Evaluation of 4-mm to 7-mm versus 6-mm prosthetic brachial-antecubital forearm loop access for hemodialysis: results of a randomized multicenter clinical trial," *J. Vasc. Surg.*, Vol. 37, pp. 143-148, 2003.

[21] F. Loth, S. A. Jones, G. P. Giddens, H. S. Bassiouny, S. Glacov, and C. K. Zarins, "Measurements of velocity and wall shear stress inside a PTFE vascular graft model under steady flow conditions," *J. Biomech. Eng.*, Vol. 119, pp. 187-194, 1997.

[22] K. Hayashi, K. Mori, and H. Miyazaki, "Biomechanical response of femoral vein to chronic elevation of blood pressure in rabbits," *Am. J. Physiol. Heart Circ. Physiol.*, Vol. 284, pp. H511-H518, 2003.

[23] E. Monos, M. Lorant, and E. Feher, "Influence of long-term experimental orthostatic body position on innervation density in extremity vessels," *Am. J. Physiol. Heart Circ. Physiol.*, Vol. 281, pp. H1606-H1612, 2001.

[24] M. Jr. Szentivanyi, G.L. Nadasy, M. Toth, V. Kopxsanyi, A. Jednakovits, and E. Monos, "Biomechanics of the saphenous artery and vein in spontaneous hypertension in rats," *Pathophysiology*, Vol. 4, pp. 295-302, 1998.

[25] E. Monos and J. Csengody, "Does hemodynamic adaptation take place in the vein grafted into an artery?," *Pflügers Arch.*, Vol. 384, pp. 177-182, 1980.

[26] R.L.R. Wesley, R.N. Vaishnav, J.C.A. Fuchs, D.J. Patel, and J.C. Jr. Greenfield, "Static linear and nonlinear elastic properties of normal and arterialized venous tissue in dog and man," *Circ. Res.* Vol. 37, pp. 509-520, 1975.